Advances in Materials and Pavement Performance Prediction – Masad et al. (Eds)
© 2018 Taylor & Francis Group, London, ISBN 978-1-138-31309-5

Analysis of the tire pressure effect on flexible pavement's responses by means of FEM and APT instrumentation

D. Clark, P. Leiva, L.G. Loría & J.P. Aguiar
LanammeUCR, San José, Costa Rica

ABSTRACT: In this research, a 3-D FEM model of a flexible pavement section was used to analyze the effect of the tire inflation pressure and load frequency on different pavement responses. The model was validated using data obtained in test tracks of an Accelerated Pavement Testing Facility (Pavelab, LanammeUCR) at the University of Costa Rica. Different actual loading conditions were measured using a contact pressure sensor and a Heavy Vehicle Simulator (HVS), to include the mapped pressures in the FEM model. Lastly, a parametric study with multiple loading scenarios was performed. Results show that higher pavement response values were obtained with higher tire pressures, in contrast, with higher load frequencies lower pavement response values were obtained. Increments of 14.62% to 67.4% were observed by changes in the load frequency, and increments between 5.1% and 10.87% were observed by changes in the inflation pressure.

1 INTRODUCTION

1.1 *Introduction*

Pavement deterioration is caused by the periodic action of different factors: environmental effects, repeated traffic loads, poor construction and poor maintenance. In this context, understanding the interaction between the vehicle tires and the pavement is required.

This research analyzes the effect of the tire inflation pressure on flexible pavement responses. The project is part of the accelerated pavement testing research line at the PaveLab (National Laboratory of Materials and Structural Models of the University of Costa Rica LanammeUCR).

A 3D FEM model of a flexible pavement section was developed and then validated with real pavement responses obtained with instrumentation embedded in the test tracks in the Pavelab facility. Finally, a parametric study was performed, varying the load conditions in the FE model.

1.2 *Test track description*

Pavelab currently has four experimental test tracks under evaluation, as shown in Figure 1. The tracks differ in layer thickness and base material properties (granular base -AC1, AC4-, and CTB -AC3, AC2-).

Each test track is instrumented with asphalt strain gauges, pressure cells, multi depth deflectometers (MDD), moisture and temperature probes. The asphalt strain gauge sensors were placed at the base/HMA interface. MDD sensors were installed at four different depths to asses each structural layer. Four thermocouples were placed in the HMA and granular base layers.

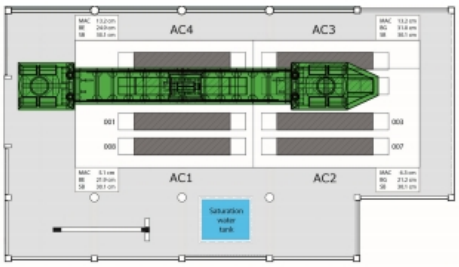

Figure 1. Test track configuration.

2 FLEXIBLE PAVEMENT MODEL

2.1 *General description*

For this study, a 3D FEM model of a flexible pavement section was developed using COMSOL Multiphysics®. Two different study cases were analyzed: 1) static load analysis, using linear elastic properties for the hot mix asphalt (HMA) layer and non-linear elastic properties for the base, subbase and subgrade materials; and 2) time dependant load analysis, using viscoelastic properties to

describe the HMA layer and linear elastic properties for the other layers.

2.2 *Model geometry*

The AC3 test track structure, as shown in Table 1, was modeled using finite element analysis. Geometric properties, such as the full depth, width and height of the model were selected based on previous studies (see Wang 2011). Specifically, a 2.5 m × 3 m × 3 m (depth, width and height respectively) structure was modeled. Domain size optimization (sensitivity analysis for the geometry) wasn't performed for this study.

In the model, two symmetry axis are applied in the horizontal plane (X-Y), as per Figure 2. Only one quarter of the model is analyzed.

Table 1. Test track structures.

Section	Asphalt concrete Thickness (cm)	Base Thickness (cm)	Subbase Thickness (cm)
AC1	5.1	21.9	30.1
AC2	6.3	21.2	
AC3	13.2	31.0	
AC4		24.9	

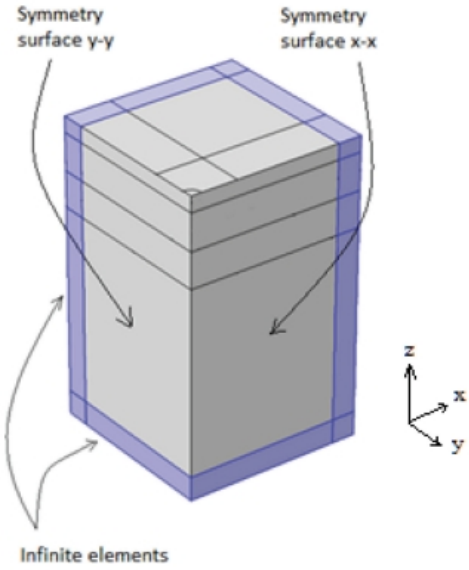

Figure 2. Quarter FE model of a flexible pavement section.

2.2.1 *FE mesh*

Brick and tetrahedrical elements with a quadratic discretization were used in the finite domain, and infinite type elements were used in the boundaries of the model. A sensitivity analysis was performed to define the mesh.

2.3 *Material characterization*

Material properties used in the FE model depend on each study condition (see section 2.1). For the static load analysis, linear elastic properties are used to describe the HMA layer and non-linear elastic properties are used for the other layers. Table 2 shows the material properties for the static load analysis.

For the time dependant analysis, viscoelastic properties are used to describe the HMA, and linear elastic properties to describe the materials in the base, subbase and subgrade layers. Table 3 shows the material properties used in the second case.

In both cases, materials are assumed to be uniform and isotropic.

2.3.1 *Non-linear properties of the supporting layers*

The May & Witzcak model (May & Witzcak 1981) is used to define the non linear modulus of this materials; the equation was calibrated in the Pavelab for materials typically used in road construction in Costa Rica. For the base and subbase, the equation has the following form:

$$M_{R1} = 1.073 * p_a * \left(\frac{\theta}{p_a}\right)^{0.376} * \left(\frac{\sigma_d}{p_a}\right)^{-0.105} \quad (1)$$

Table 2. Material properties used for the static load analysis.

Material	Modulus	Poisson ratio
HMA	3800 MPa	0.3
Base/subbase	Equation (1)	0.3
Subgrade	Equation (2)	0.45

Table 3. Material properties used for the time dependant analysis.

Material	Modulus	Poisson ratio
HMA	Prony series (section 2.3.2)	0.3
Base	170 MPa	0.3
Subbase	140 MPa	0.3
Subgrade	70 MPa	0.45

And for the subgrade:

$$M_{R2} = 0.366 * p_a * \left(\frac{\theta}{p_a}\right)^{0.337} * \left(\frac{\sigma_d}{p_a}\right)^{-0.350} \quad (2)$$

where p_a = atmospheric pressure (kPa); θ = first stress invariant (kPa); and σ_d = deviatoric stress (kPa). The results of this equations are given in MPa.

2.3.2 *Linear viscoelasticity of the HMA*

Prony series coefficients represent the modulus of a viscoelastic material in terms of the relaxation time (see Tzikang 2000). In this study, Prony series were used to describe the linear viscoelastic behavior of the HMA material. Dynamic modulus test data obtained at LanammeUCR was used to calibrate the Prony coefficients.

2.4 *Load modeling*

The tire-pavement contact stress distribution was measured with a pressure mapping device under the Heavy Vehicle Simulator (HVS) dual tire configuration. Inflation pressures between 552 kPa–793 kPa and loads between 40 kN–60 kN were measured under static loading condition.

3 RESULTS

The model was validated through a comparison between FE model results, APT test data and results obtained based on MultiLayer Elastic Theory (MLET). Four different responses were analyzed: the displacement at the surface of the model (under the load center), the vertical strains at the middle of each layer, the radial strains at the bottom of the HMA, and the shear strains in the HMA layer.

Figure 3 shows the radial strains at the bottom of the HMA layer in the traffic direction. As observed, APT test data has a very good fit with data obtained from the FE model (in this case, a static load and non linear properties for the base, subbase and subgrade were used). The MLET results were computed with backcalculated moduli from the Pavelab test tracks.

With the validated model, a parametric analysis was performed. The responses were analyzed, varying the tire inflation pressure and the load frequency.

Figure 4 shows the vertical strain results at the middle of the asphalt mixture. The effect of inflation pressure under the load can be observed: Figure 4a shows the results for frequency values between 0.1 Hz and 25 Hz, using a inflation

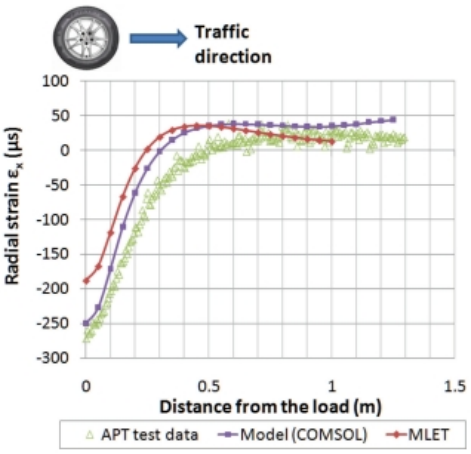

Figure 3. Radial strain at the bottom of the HMA layer under the load.

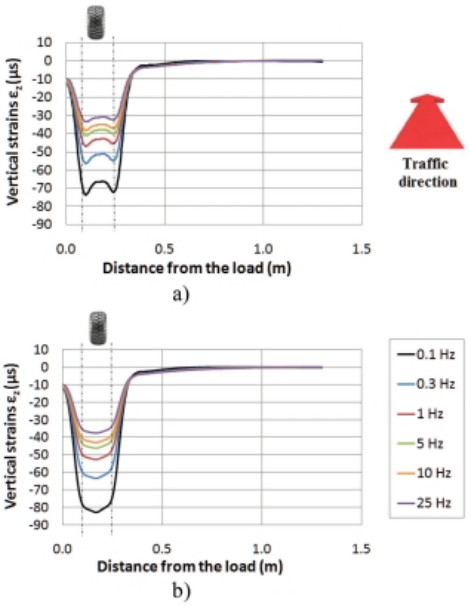

Figure 4. Vertical strain in the middle of the HMA layer; a) Applied load of 60 kN and tire pressure of 552 kPa, b) Applied load of 60 kN and tire pressure of 793 kPa.

pressure of 552 kPa. For this condition, the critical response occurs at the edge of the load ribs. In Figure 4b, same frequencies were applied, with a higher inflation pressure value (793 kPa). In this

Table 4. Prony series used in the FE model.

G_0 (MPa)	ρ (kg/m³)	Temp. (°C)
1.66	2380.41	21
I	Gi (MPa)	τi (s)
1	1193.70	1.0E-06
2	1889.46	1.0E-04
3	3069.62	1.0E-02
4	2489.93	1
5	720.18	1.0E+02
6	80.26	1.0E+04
7	20.27	1.0E+06

Table 5. Measured responses variation by changes of the tire inflation pressure and the load frequency.

Responses		Maximum obtained value	Maximum variation (%) by changes of: Tire pressure	Load frequency
Surface displacement (mm)		0.71	5.79	14.62
Strains in the HMA layer (μs)	Radial	246	6.1	34.35
	Shear	83.7	5.1	67.4
	Vertical	−82.8	10.87	53.85

case, the critical response occurs at the middle of the load rib.

As expected, higher response values were obtained with the highest inflation pressure (793 kPa). However, it can be noted that the effect of the load frequency on the responses in the HMA layer appears to be more critical than the effect of the tire inflation pressure. This occurs for all the measured responses, as seen in Table 5.

4 CONCLUSIONS AND RECOMMENDATIONS

The drawn conclusions are based on the evaluated sections and the assumptions used in this study.

The findings of the study can be summarized as follows:

- The load magnitude and the inflation pressure have a different effect on the contact stress distribution of the tire footprint. As the tire pressure increase, the contact stress increase in the middle section of the tire footprint. Inversely, as the applied load magnitude increase, the contact stress increase in the outer sections of the tire footprint.
- Under static loading conditions, measurements show that vertical contact stresses have a convex shape along the contact length (parallel to the transit direction). This shape flattens in its middle section as the load increases. Contact pressures appear to reach a maximum value similar to the tire inflation pressure.
- In the outer ribs the same convex shape was observed. However, for a inflation pressure of 552 kPa and a load of 60 kN, overpressures (maximum contact pressures exceeding the magnitude of the tire inflation pressure) were observed in the tire footprint.
- The tire inflation pressure has a small effect on pavement displacement. Although variations were observed in the results, the maximum observed variation was 5.79% between different inflation pressures.
- For the radial and vertical strains, the critical response values (246 and −82.8 microstrains respectively) were obtained under the tires.
- Highest values of shear strain (ε_{YZ}) were observed at the outer side of the edge ribs at a depth of approximately 1 inch in the HMA layer. The critical value (83.7 microstrain) was obtained with a pressure of 552 kPa, most likely because the highest values of contact stress at the edge ribs were obtained with this pressure.
- Increments of 14.62% to 67.4% were observed by changes in the load frequency, and increments between 5.1% and 10.87% were observed by changes in the inflation pressure. Been the shear strain in the HMA the most affect response by variations in the load frequency, and the vertical strain by variations in the inflation pressure.
- The effect of the inflation pressure on the resilient modulus distribution in the base, subbase and subgrade layers is almost negligible.

REFERENCES

Aguiar-Moya, J.P., et al. PaveLab and heavy vehicle simulator implementation at the National Laboratory of Materials and Testing Models of the University of Costa Rica. Advances in pavement design through full-scale accelerated pavement testing, 2012, p. 25.

Burmister, D.M., 1943. The Theory of Stresses and Displacements in Layered Systems and Applications to the Design of Airport Run ways. Proceedings, Highway Research Board, Vol.23, pp. 126–144.

Burmister, D.M., 1945. The General Theory of Stresses and Displacements in Layered Soil Systems. Journal of Applied Physics, Vol. 16, pp. 84–94,126–127, 296–302.

Casey, Dermot B.; Grenfell, James R.; Airey, Gordon D. 3-D longitudinal and transverse cracking and the influence of non-uniform contact pressure on the stress intensity.

Christensen, R.M. (1969). Viscoelastic properties of heterogeneous media. Journal of the Mechanics and Physics of Solids, 17(1), 23–41.

Chandrupatla, Tirupathi R., et al. Introduction to finite elements in engineering. Upper Saddle River, NJ: Prentice Hall, 2002.

Hajj, E., Thushanthan, P., Sebaaly, P., & Siddharthan, R. (2012). Influence of tire-pavement stress distribution, shape, and braking on performance predictions for asphalt pavement. *Transportation Research Record: Journal of the Transportation Research Board*, (2306), 73–85.

Huang, Y.H., 1993. Pavement analysis and design.

Leiva-Villacorta, Fabricio; Aguiar-Moya, Jose Pablo; Loría-Salazar, Luis Guillermo. Accelerated pavement testing first results at the Lanammeucr APT facility. 2014.

May, Richard W.; Witczak, Matthew W. Effective granular modulus to model pavement responses. 1981.

Seed, Harry Bolton; Chan, C.K.; Lee, Clarence Edgar. Resilience characteristics of subgrade soils and their relation to fatigue failures in asphalt pavements. En International Conference on the Structural Design of Asphalt Pavements. Supplement University of Michigan, Ann Arbor. 1962.

Tzikang, C. (2000). Determining a Prony series for a viscoelastic material from time varying strain data.

Uzan, Jacob. Characterization of granular material. Transportation research record, 1985, vol.1022, no 1, p. 52–59.

Wang, Hao. Analysis of tire-pavement interaction and pavement responses using a decoupled modeling approach. University of Illinois at Urbana-Champaign, 2011.

Witczak, M.W.; Uzan, J. The Universal Airport Design System, Report I of IV: Granular Material Characterization. Rep. to Department of Civil Engineering, 1988.